Ion-mediated desorption of asphaltene molecules from carbonate and sandstone structures

To cite this article: Pouyan Ahmadi *et al* 2022 *Mater. Res. Express* **9** 065101

View the article online for updates and enhancements.

Materials Research Express

PAPER

Ion-mediated desorption of asphaltene molecules from carbonate and sandstone structures

Pouyan Ahmadi[1] , Mohammadreza Aghajanzadeh[2,3], Hamidreza Asaadian[4,*] , Armin Khadivi[5] and Shahin Kord[6]

1   Department of Hydrogeology, Helmholtz-Centre for Environmental Research, UFZ, Germany
2   Department of Civil Engineering, Monash University, Melbourne, Australia
3   Department of Petroleum Engineering, Amirkabir University of Technology, Tehran, Iran
4   Norwegian University of Science and Technology (NTNU), Department of Geoscience and Petroleum, Trondheim, Norway
5   Technical University of Berlin, Berlin, Germany
6   Ahwaz Faculty of Petroleum, Petroleum University of Technology, Ahwaz, Iran
*   Author to whom any correspondence should be addressed.

E-mail: hamidreza.asaadian@hotmail.com and hamidreza.asaadian@ntnu.no

Abstract

As more and more oil recovery scenarios use seawater, the need to identify the possible mechanisms of wettability state changes in oil reservoirs has never been greater. By using molecular dynamics simulations, this study sheds light on the effect of ions common to seawater (Ca^{2+}, K^+, Mg^{2+}, Na^+, Cl^-, HCO^{3-}, SO_4^{2-}) on the affinity between silica and carbonate as the traditional rock types and asphaltene molecules as an important contributing factor of reservoir oil wetness. In the case of carbonate and silica being the reservoir rock types, the measured parameters indicate good agreement with each other, meaning that (HCO_3^- & SO_4^{2-}) and (Na^+ & Cl^-) ions reached maximum bonding energies of (25485, 25511, 4096, and -4093 eV, respectively). As with the surface charge density measurements, the results of the non-bonding energies between the individual atomic structures agree with those from the simulation cell. In the presence of a silica surface, the radial distribution function (RDF) results determine that the peak of the maximum value for the distribution of the ions is 4.2. However, these values range from 3 to 6.6, suggesting that different ions perform better under the influence of carbonate rock. As these ions are distributed in the simulation box along with the adsorption domain, the conditions for sequestering asphaltene from the rock surface are made ideal for dissolution and removal. At equal ion strength, measuring the distance between the center of mass of rocks and asphaltene structures reveals a maximum repulsion force of 22.1 Å and a maximum detachment force of 10.4 Å in the presence of SO_4^{2-} and Na^+ ions on carbonate and silica surfaces.

1. Introduction

Smart water flooding has been proven to be one of the most successful methods for improving oil recovery due to the impact of water chemistry and salinity on reservoir fluid-fluid and rock-fluid interactions [1–5]. It has been shown that the recovery of crude oil can be improved by manipulating the injection water [6–9]. Although numerous studies have been conducted over the last two decades to study the effect of smart salinity water flooding on the improvement of crude oil recovery in carbonate and sandstone reservoirs, the underlying mechanisms have not been completely revealed [2]. Multi-ion exchange (MIE), double-layer expansion (DLE), wettability alteration, and pH effect are the most important mechanisms that have been widely reported in the literature. Among these mechanisms, wettability alteration from oil-wet to water-wet is a widely accepted mechanism in this flooding method [10–17].

The wettability of the pore surface plays a vital role in the displacement of the crude oil by water. The wettability state of the reservoir rock surface can be attributed to the adsorption of polar components from crude

oil at the mineral surfaces [18–22]. It is generally accepted that underground reservoirs are saturated with formation brine before oil migrates into their rock pores. After the drainage of water by crude oil from the porous media, the reservoir wettability may become less water-wet or even oil-wet because of the adsorption of heavy components of crude oil onto rock surfaces. The main mechanisms by which crude oil compounds may adsorb onto pore surfaces include surface precipitation, polar interactions, and acid/base and ion binding interactions [18, 23, 24].

Asphaltenes are the most polar fraction in crude oil [25, 26]. The adsorption of asphaltenes on mineral surfaces is an important element of wettability changes toward oil-wet conditions and can have a strong negative impact on rock properties. Asphaltenes are polycyclic aromatic hydrocarbons (PAHs) consisting of a sheet-like structure of interlocked heterocyclic aromatic rings attached to hydrocarbon chains and containing both polar and non-polar species [27]. In addition, heteroatoms such as oxygen, sulfur, and nitrogen atoms and trace amounts of metals such as Fe, Ni, and V in asphaltene molecules make these molecules the most polar and complex components of crude oil [28]. Changing the thermodynamic conditions may cause the precipitation and adsorption of asphaltene onto the rock surface during the production and transportation of crude oil. The adsorption of precipitated asphaltenes onto the rock surface can lead to formation damage in oil reservoirs by reducing the effective oil permeability [29–31].

Many researchers have investigated the adsorption/desorption process of asphaltene molecules on and from rock surface [31–36]. It was found that precipitated asphaltene molecules on the rock surface can be adsorbed in nanofluids containing metal oxide nanoparticles, such as TiO_2, SiO_2 and Fe_2O_3 [30, 37, 38]. Other experimental and modeling studies have revealed that the injection of modified brine during the EOR process could desorb asphaltene molecules and other polar components of crude oil from the mineral surfaces and alter the wettability of the pore wall to less oil wet, resulting in improved oil recovery [7, 39–42]. Ligthelm *et al.* showed that a decrease in salinity increased the expansion of the diffuse double layer between the rock and oil interfaces, facilitating the release of organic materials [11]. Yang *et al.* studied the desorption of asphaltenes from quartz crystals in the presence of an electrolyte. They used a quartz crystal microbalance with dissipation (QCM-D), atomic force microscopy (AFM), and contact angle to measure the amount of desorbed asphaltenes. They found that desorption occurred when the rock surface was exposed to a saline solution. This is mainly because the charge density of both the surfaces of oil-water and solid-water was promoted and the electrostatic repulsions increased [43].

Despite extensive experimental and modeling studies on the effect of salinity on the adsorption/desorption of asphaltene molecules from mineral surfaces, the exact mechanism that occurs at the atomic scale still needs to be investigated in more detail; hence, the present work has concentrated on checking the influence of ions on the absorbance tendency of polar asphaltene molecules on the surface of sandstone and carbonate rocks under reservoir conditions. Hence, molecular dynamics simulations were used to understand the behavior of asphaltene molecules upon exposure to cations and anions (i.e., Ca^{2+}, K^+, Mg^{2+}, Na^+, Cl^-, HCO_3^-, SO_4^{2-}) available in smart water (salinity $\leqslant$ 5000 ppm) in the presence of carbonate and sandstone rock types [44]. The LAMMPS (stable release) software was used as the simulation tool, and all numerical calculations were crunched using this computational package. All investigation methods, such as surface charge density measurement, radial distribution function (RDF), discretizing of bonding and non-bonding energies, and measuring the asphaltene detachment distance, have proved the importance of ion types on the fate of asphaltene molecules that are stuck to the rock surface in reservoirs.

2. Computational method

2.1. Force field and relative parameters

The present work employs molecular dynamics (MD) simulations to investigate the precipitation of asphaltene on carbonate and sandstone structures in the presence of brine at a defined temperature and pressure. MD simulation is known as a computational method to estimate the dynamic translocation of particles considering the underlying concept of intermolecular interactions at the atomic scale. In addition to the molecular interaction for a specific time interval (time step), this method can provide an exact insight into the particle transformation of the structures. In this method, Newton's law, which is a numerically solving method, determines the particle trajectories. Likewise, the interaction between the particles and their interatomic energies is often computed using force fields in the system. In this study, **L**arge-scale **A**tomic/**M**olecular **M**assively **P**arallel **S**imulator (LAMMPS) software was used as a simulation tool, and the entire calculation of asphaltene deposition on carbonate and sandstone structures was implemented by this computational package using the Lennard Jones (LJ) potential [45]. This software was developed and released by Sandia National Laboratories (SNL). Simulations of this research were carried out in the following steps, as mentioned previously:

Table 1. The ε and σ parameters for non-bond interactions in simulated atomic structure [45].

	ε (kcal/mol)	σ (Å)
C	0.1450	3.9800
H	0.0100	3.20000
O	0.4150	3.71
S	0.3050	4.24
N	0.4150	3.9950
Ca	0.0500	3.4720
Si	0.0950	4.4350
Cl	0.3050	3.9150
F	0.3050	3.2850
K	0.3050	3.398
Mg	0.111	2.692
Na	0.5	3.144

Step 1: In this step, the preliminaries of the simulation are set up, such as units, boundary conditions, dimensions, bond type, atom location, and structure style. In the following simulations, the units were adjusted real, the boundary condition was periodic, and the atomic structure was full.

Step 2: In the next step, atoms and molecules were introduced into the simulation environment. After packing molecules with another software named Packmole and obtaining their data files, they were presented as input to the designated simulation cell by the read data command. Furthermore, specific groups of atoms (i.e., Ca^{2+}, K^+, Mg^{2+}, Na^+, Cl^-, HCO_3^-, SO_4^{2-}) were assigned and distinguished with unique names by group commands to achieve better control over them during simulations. In this stage, everything is well defined and the software is ready to start the simulation.

Step 3: In the last step, an approximate velocity must be estimated to minimize the convergence time by the velocity command before reaching system stability. The more related system velocity according to the system convergence temperature was estimated so that the computational time of the software used reached its minimum as much as possible. The convergence temperature was set to 60°C or 333.15 K for all scenarios to resemble reservoir conditions.

Pairstyle commands outline interactions (potential of forces) between atoms and molecules, such as intermolecular, bond, and nonbonding energies. All interaction calculations were based on the Lennard-Jones equation in the following simulation work.

Lennard-Jones presented the first formula for this relationship in 1924 [45]. The following equation is called the Lennard (LJ) potential.

$$\mathrm{U}(\mathbf{r}) = 4\varepsilon\left[\left(\frac{\sigma}{\mathbf{r_{ij}}}\right)^{12} - \left(\frac{\sigma}{\mathbf{r_{ij}}}\right)^{6}\right]\mathbf{r} < \mathbf{r_c} \tag{1}$$

where U(r) represents the Dreiding force field [45], is the non-bond interaction, ε is the depth of the potential well, σ is the distance at which the potential is 0, and r_{ij} is the distance between the atoms and molecules. This equation can theoretically estimate the interactions between a pair of particles (atoms and molecules). Table 1 presents the scale of the length and energy parameters of various atoms in the simulated structures. The cutoff radius was set to 12 Å for interactions between pairs of particles. Furthermore, Coulomb interaction was implemented for the simulated structures using the following equation:

$$E(\boldsymbol{r}) = \frac{CQ_iQ_j}{\varepsilon\,\boldsymbol{r}}\boldsymbol{r} < \boldsymbol{r_c} \tag{2}$$
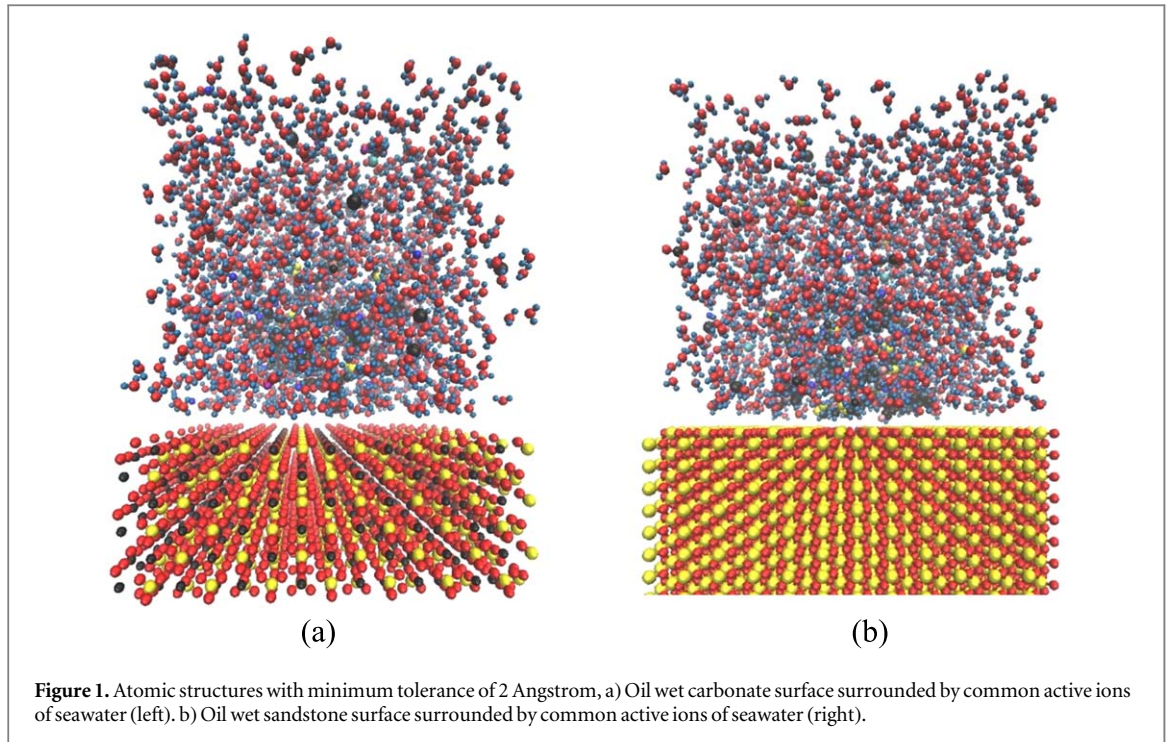
Where C is the energy-conversion constant, and ε represents the dielectric constant. Q_i and Q_j are the charges on two atoms. The cut-off radius is set to 10 Å for this type of non-bonding interaction, and all atomic structures with distances larger than the cut-off radius will not be taken into account in the numerical calculations ($\boldsymbol{r} < \boldsymbol{r_c}$).

The bond and angle strengths for the Dreiding potential are defined by a simple harmonic oscillator equation as follows:

$$E = 1/2K_r(r - r_\theta)^2 \tag{3}$$

$$E = 1/2K_r(r - r_0)^2 \tag{4}$$

where K_r and K_θ are harmonic oscillator constants, and r_0 and θ_0 represent the length of the atomic bond and equilibrium value of the angle, respectively. In this work, the harmonic oscillator constants were adjusted to 700 ((kcal/mol)/Å²) and 100 ((kcal/mol)/degree²) for K_r and K_θ, respectively. The atomic bond lengths and

Figure 1. Atomic structures with minimum tolerance of 2 Angstrom, a) Oil wet carbonate surface surrounded by common active ions of seawater (left). b) Oil wet sandstone surface surrounded by common active ions of seawater (right).

equilibrium values of the angles for each bonded interaction are listed in table 2 [45]. Furthermore, the dihedral interactions in these simulations were based on previously reported bonding interactions. These bonding interactions were calculated using the harmonic equation, and the coefficients were selected from the Dreiding force field [45]:

$$E = K(1 + dcos(n\varnothing)) \qquad (5)$$

where K is the harmonic oscillator constant, d $= +1$ or -1 and n is the integral number [45].

In addition, the Dreiding force field is used for rock-asphaltene, rock–ion, ion–asphaltene, and rock-fluid interactions. Moreover, Newton's second law at the atomic level was used for computations of the particle motion through the simulation time. The following formula shows the gradient of the potential relation:

$$F_i = \sum_{i \neq j} \boldsymbol{F_{ij}} = m_i \frac{d^2\boldsymbol{r_i}}{dt^2} = m_i \frac{d\boldsymbol{v_i}}{dt} = -grad \; V(r_{ij}) \qquad (7)$$

The association of previous relations is performed using the velocity-Verlet algorithm to integrate Newton's law as follows:

$$v(t + \delta t) = v(t) + a(t)\delta t \qquad (8)$$
$$v(t + \delta t) = r(t) + v(t)\delta t \qquad (9)$$

In these two relations, **r** $(t + \delta t)$ and **v** $(t + \delta t)$ are the final position and velocity of the atoms (respectively) and **r** (t) and **v** (t) are the initial rates of these mechanical parameters.

2.2. Designed atomic structures of molecules in the simulation cell

The designed simulation cells containing carbonate and sandstone surfaces along with the ions and asphaltene molecules were adjusted according to the Dreiding force field parameters to define the atomic structures and force field. Figure 1 shows the frame in which the studied ions were randomly arranged by Packmole software (version 20.010) in such a way that the ion strength for all scenarios was kept constant with a view to having an exact comparison of ion impact on the way rock that the asphaltene molecule deals with rock surfaces in all cases. In support of this idea, 10 asphaltene molecules considered in all scenarios and 100 of each ion were randomly distributed in the designed cell, and the effect of the mixture of all ions was examined to observe the behavior of asphaltene. Moreover, because most of the carbonate and sandstone rock constituents are made of SiO_2 and $CaCO_3$, respectively, and to eliminate the impact of impurities, the pure structures of each rock type were considered in all simulations.

In all scenarios, water molecules were also added to the cells considering their real number, which was proportional to the designed simulation cell volume. The pressure and temperature were adjusted to 60°C and 2500 psi, respectively, to make the situation more thermodynamically similar to real reservoir conditions. In this study, the asphaltene molecule is precipitated due to thermodynamic disturbance and is not soluble in the water

Table 2. The equilibration distance/ angle for bond strength and bond-angle bend in MD simulations [45].

Parameter	r_0 (Å)	θ_0 (degree)
C-C bond	1.530	—
N-F bond	1.371	—
C-H bond	1.090	—
C-N bond	1.462	—
C-O bond	1.420	—
C-S bond	1.800	—
C-Cl bond	1.757	—
H-N bond	1.022	—
H-O bond	0.980	—
H-S bond	1.360	—
O-S bond	1.690	—
O-Si bond	1.587	—
S-S bond	2.070	—
C-C-C	—	109.471
C-C-F	—	109.471
C-C-H	—	109.471
C-C-N	—	109.471
C-C-O	—	109.471
C-H-S	—	180.000
C-N-C	—	106.700
C-N-H	—	106.700
C-S-C	—	92.100
C-S-H	—	92.100
C-S-O	—	92.100
C-S-S	—	92.100
H-C-H	—	109.471
H-C-N	—	109.471
H-C-S	—	109.471
H-O-H	—	104.51
H-S-H	—	92.100
H-S-O	—	92.100
H-S-S	—	92.100
N-C-O	—	109.471
O-S-S	—	92.100
O-Si-O	—	109.471
S-C-S	—	109.471
S-O-S	—	104.51
Si-O-Si	—	104.51

bulk, which implies that the asphaltene molecule detachment could either intensify or alleviate under the influence of what happens in the brine solution. Figure 2 shows the structure of the polar asphaltene molecules, which was used to check the effect of their tendency to be adsorbed on the rock surfaces. The asphaltene structure belongs to one of the southern Iranian oilfields, which contains heteroatoms (nitrogen, oxygen, and sulfur) as the electronegative part of the asphaltene molecule.

3. Results and discussion

This study investigated a wide variety of possible aspects that could explain the interaction tendency between rock, asphaltene molecules, and ions. The appropriate parameters that could reveal the affinity between individual structures in an atomic-scale simulation cell, including bonding and non-bonding energies, surface charge density, asphaltene angle on the rock, ion density inside the simulation cell, radial distribution function (RDF), and displacement of the atomic structure center, will be discussed in order to gain a thorough understanding of the behavior of asphaltene molecules on carbonate and sandstone surfaces. These surfaces have been selected because they comprise the majority of conventional and unconventional rock types worldwide.
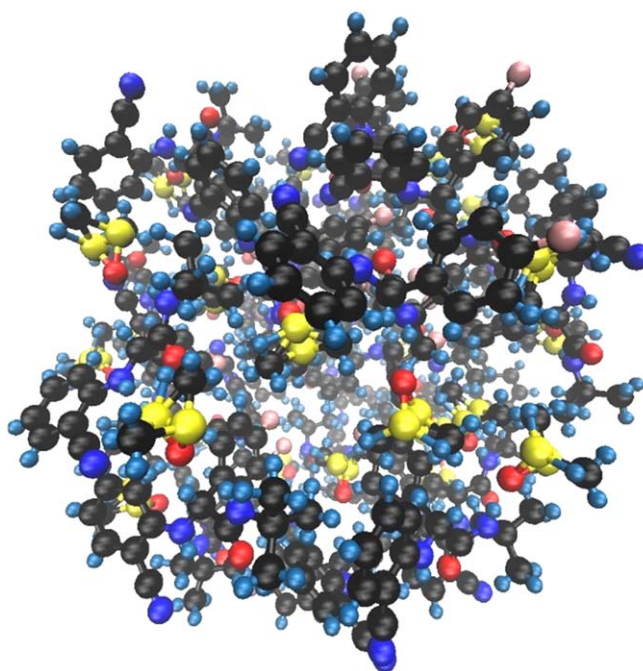
Figure 2. Asphaltene molecule used in the simulations.

Table 3. Bonding and non-bonding energies of the simulation cell for carbonate and sandstone surfaces along with ions as well as asphaltene molecules.

	Carbonate rock		Sandstone	
Ion type	Bonding energy (eV)	Non-bonding nergy (eV)	Bonding energy (eV)	None-binding energy (eV)
Ca^{2+}	26572	25423	1066441	3867-
SO_4^{2-}	61121	25511	1066354	36803-
Cl^-	60600	24332	1066341	4093-
HCO_3^-	60913	25485	1066270	36789-
K^+	60953	25436	1066343	4112-
Mg^{2+}	61148	25405	1066355	4116-
Na^+	45591	25434	1066356	4096-
All ions	45442	25050	1066805	4187-

3.1. Bonding and non-bonding energies of the simulated structures

Intermolecular interactions between the atoms of an individual molecule can also be described using bonding and non-bonding energies. Considering the defined LJ potential and different values that were assigned to the bond and angle strengths, the higher the positive values of the bonding and non-bonding energies, the more repulsive forces exist between the atomic and molecular structures. The negative values imply that the adsorption forces will rule the simulation cell so that the density of the structures will be increased where the attractive forces are dominant; therefore, the chances of interactions occurring will be boosted.

Table 3 provides the data of the bonding and non-bonding energies of the simulation cell for carbonate and sandstone surfaces, along with ions and asphaltene molecules. The positive nonbonding energy for the simulation cell with the carbonate surface indicates a repulsive dominant interaction compared to that of the sandstone surface. The presence of SO_4^{2-} and HCO_3^- in the simulation cell led to maximum non-bonding energies with values of 25485 eV and 25511 eV, respectively, while the maximum energy in the sandstone surface occurred when Cl^- and Na^+ were available in the simulation cell. However, adding all the ions in the cell resulted in the minimum values of non-bonding energy in both cases (i.e., carbonate and sandstone surfaces). It is well known that non-bonding energy can only inspire the presence of repulsive forces between surfaces and asphaltene molecules, and the amount of this energy depends on other parameters, such as the patterns in which

Table 4. The angle between rock slabs and asphaltene molecules in presence of water molecules and ions .

Ion Type	Angle with carbonate surface (Θ)	Angle with sandstone surface (Θ)
H_2O	88	84
Ca^{2+}	89	93
$SO4^{2-}$	86	91
Cl^-	84	88
HCO_3^-	92	90
K^+	91	91
Mg^{2+}	88	84
Na^+	85	83
All ions	84	80

Table 5. Effect of water molecules on the angle between rock slabs and asphaltene molecules in presents of individual ions.

Ion Type	Angle with carbonate surface (Θ)	Angle with sandstone surface (Θ)
$H_2O + Ca^{2+}$	91	90
$H_2O + SO4^{2-}$	88	92
$H_2O + Cl^-$	90	93
$H_2O + HCO_3^-$	88	92
$H_2O + K^+$	92	87
$H_2O + Mg^{2+}$	85	89
$H_2O + Na^+$	91	90
$H_2O + $ All ions	92	90

Table 6. Surface charge density variation for carbonate and sandstone.

Ion Type	carbonate surface charge density (Cmm^{-3})	sandstone surface charge density (Cmm^{-3})
Ca^{2+}	1.032	1.521
SO_4^{2-}	0.821	1.539
Cl^-	1.022	1.519
HCO_3^-	0.871	1.555
K^+	1.024	1.52
Mg^{2+}	1.022	1.532
Na^+	0.985	1.541
All ions	1.232	1.736

ions will be distributed in the simulation cell as well as the initial distance of the different molecules at the beginning of the simulation time. Generally, it can be stated that the positive values of the non-bonding energy on the carbonate surface indicate the dominance of repulsive forces between asphaltene molecules and the carbonate surface. Hereafter, *all ions* in the following tables imply all the investigated ions (i.e., Ca^{2+}, K^+, Mg^{2+}, Na^+, Cl^-, HCO_3^- , and SO_4^{2-}).
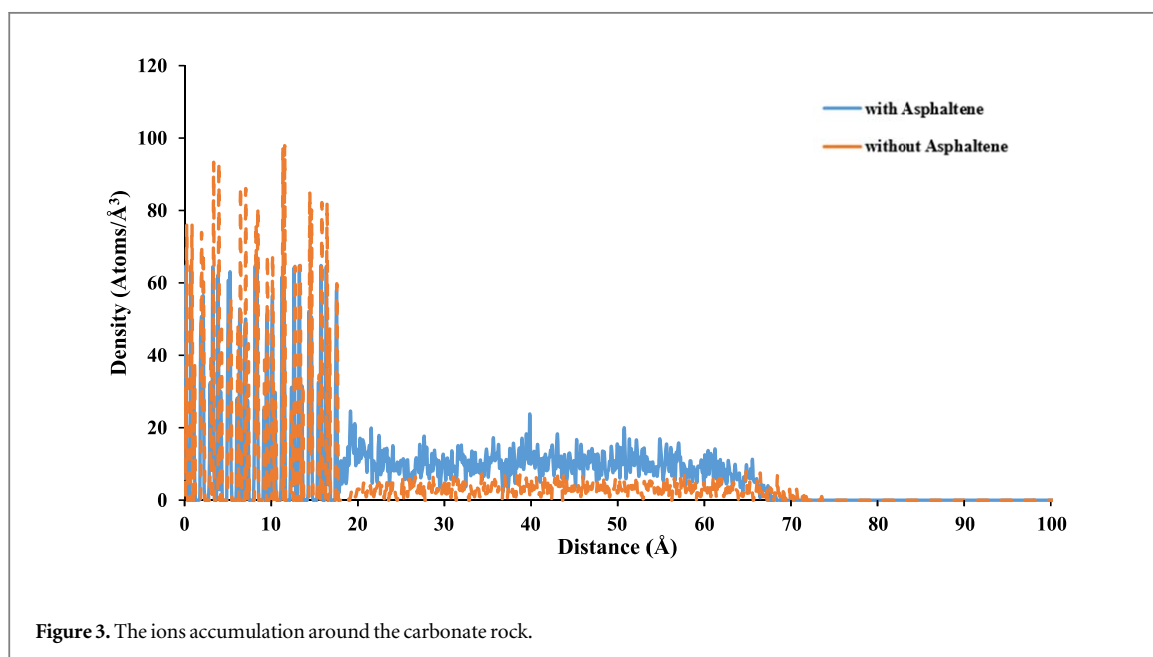
3.2. The angle between asphaltene center of mass and rock surfaces

In aquatic environments, asphaltene molecules are surrounded by polar water molecules. To examine whether the polarity of water molecules affects the behavior of asphaltene molecules, the angle between the center of mass of the asphaltene rock surface slab was measured for three different scenarios.

A) Asphaltene molecules in the presence of only water molecules available in the simulation cell (table 4).

B) Asphaltene molecules in the presence of each ion individually; therefore, the water molecules were omitted (table 4).

C) Asphaltene molecules along with water molecules and ions (table 5).

Table 7. The locations of maximum peak values for the ions distribution and the atoms of asphaltene structure.

| | in presence of sandstone | | | in presence of carbonate | | |
| | coordinate (Å) first peak | | | coordinate (Å) first peak | | |
Ion Type	Ion peak in absence of Asphaltene	ion peak in presence of Asphaltene	asphaltene peak in presence of ions	Ion peak in absence of Asphaltene	ion peak in presence of Asphaltene	asphaltene peak in presence of ions
Ca^{2+}	4	4.2	4.2	3.6	3	5.4
SO_4^{2-}	3.8	4.2	4.2	2.2	4.2	5.4
Cl^-	4	4.2	4.2	2.2	4.2	5.4
HCO_3^-	3.8	4.2	4.2	2.8	6.6	5.4
K^+	3.8	4.2	4.2	4.2	4.2	5.4
Mg^{2+}	4	4.2	4.2	4	4.2	5.4
Na^+	4	4.2	4.2	4	4.2	5.4

Figure 3. The ions accumulation around the carbonate rock.

Tables 4 and 5 and provide the data of the mentioned steps, since the obtained data are not following any logical trend to represent a meaningful deviation from the case that only water exists in the simulation cell and all the data are almost the same, the fact can be concluded that the observed fluctuation of angle values are attributed only to the randomly motion of the water molecules and the performance of each ion to affect the wettability state of the rock slabs will not be interrupted by the polar water molecules and those slight differences of angle values are correspond to the Brownian motions of water molecules and momentum theory.

3.3. Surface charge density of carbonate and sandstone surfaces

Coulomb interactions as another side of non-bonding interactions is the other parameter that has been looked into it in order to find the influences of different ions on the surface charge density changes. Considering the data in table 6, the positive numbers indicate the adsorption interaction of the present structures in the simulation cell. The inverse relationship of the Coulomb interaction with the distance between two specific atomic structures demonstrates the lower affinity of the carbonate and sandstone surfaces to attract asphaltene molecules rather than the simulation cell, which contains each ion individually. When all the ions are available in the simulation cell, the charge densities are 1.232 and 1.736 for carbonate and sandstone structures, respectively, whereas the surface charges are at the minimum states with SO_4^{2-} and Cl^-, respectively, in the simulation cell with charge densities of 0.821 and 1.519, respectively.

3.4. Radial distribution functions of simulated ions in simulation cells

The distribution of ions under the effect of their affinity for being attracted or repelled by other atomic structures is arranged. Considering all the evidence that implies the effectiveness of all ions participating in the process of asphaltene detachment from the rock surfaces, such as bonding and non-bonding energies and surface charge
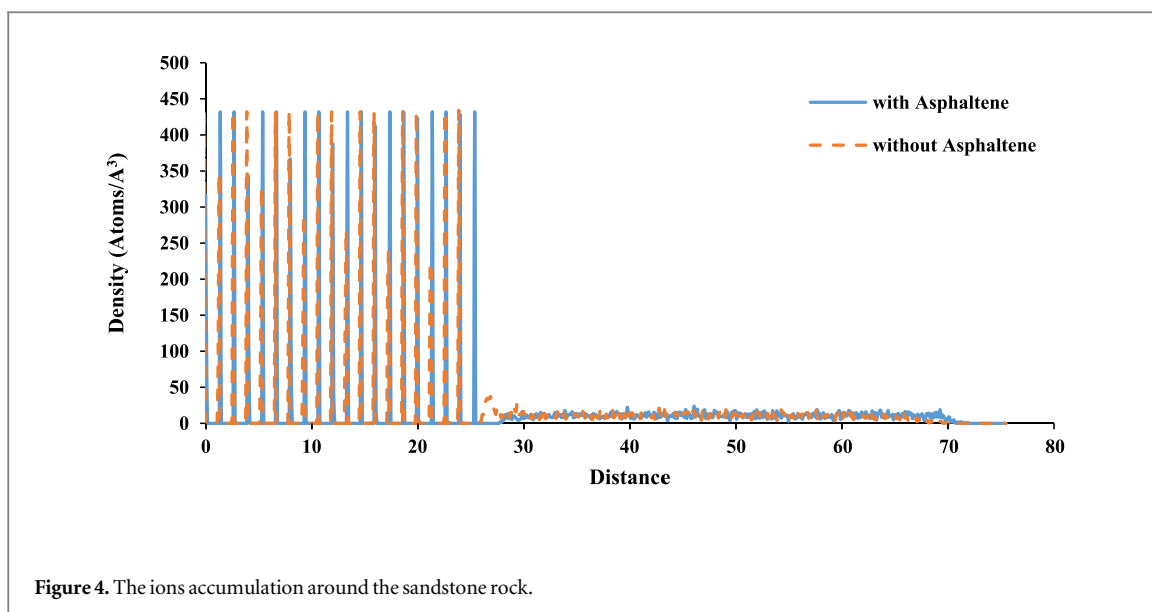
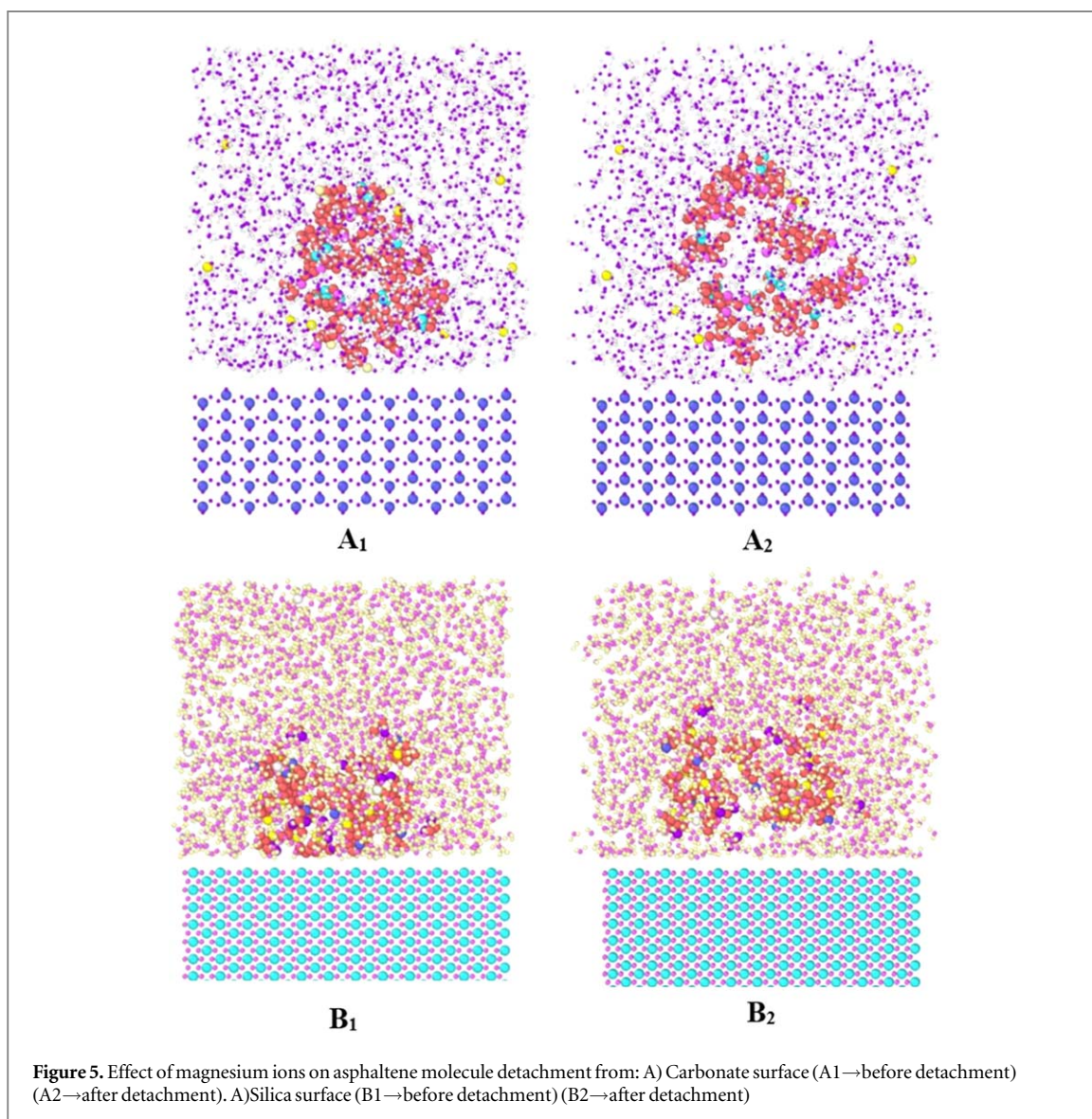**Figure 4.** The ions accumulation around the sandstone rock.

Figure 5. Effect of magnesium ions on asphaltene molecule detachment from: A) Carbonate surface (A1→before detachment) (A2→after detachment). A)Silica surface (B1→before detachment) (B2→after detachment)

Table 8. The detachment information of asphaltene molecule under the effect of common ions in the smart water.

Ion Type	Distance between asphaltene molecule and carbonate surface (Å)	Distance between asphaltene molecule and sandstone surface (Å)
Ca^{2+}	19.8	9.7
SO_4^{2-}	22.1	9.3
Cl^-	19.8	9.8
HCO_3^-	21.6	9.1
K^+	19.1	9.7
Mg^{2+}	19.8	9.5
Na^+	20	10.4
All ions	16.6	7.1

density, this scenario was designed in such a way that the influence of asphaltene molecules could be monitored. As is evident from the data provided in table 7, adding asphaltene molecules to the simulation cell leads to a decrease in the attraction forces between the rock surfaces, and the reason for such a difference lies in the attraction of ions by various atoms in the asphaltene molecule. As table 7 shows, in the presence of sandstone surface, the equal values of 4.2 for all the atomic structures, show an equal distribution of ions in the simulation cell, and its comparison with the respective values attributed to the ions in the presence of carbonate rock reveals that these ions have a better performance compared to the other case, so that their values vary from 3 to 6.6, which demonstrates a better ion distribution and dissolution and consequently better asphaltene detachment.

The density of all ions, taking into account the effects of rock surfaces and asphaltene molecules, are plotted as the RDF in figures 3 and figure 4. A comparison of these two situations clearly shows that the attraction between the ions and asphaltene molecules will affect the ion distribution, so that adding asphaltene to the system causes ions to be stabilized at a distance greater than in the case of having the same situation without asphaltene molecules. Therefore, the asphaltene inside the system should not expect all the ions to approach the rocks as close as possible to the simulation cells empty of asphaltene molecules.

The cut-off radius was considered to be equal to 12 Å to solve the LJ potential function for all the atoms that exist inside the simulation cell, which means that all the ions with a distance greater than the determined cut-off radius will not exert any force on each other. A deeper look into these reveals that in the case of an asphaltene molecule in the system, the ions and the surface of rocks fall apart more than in the case with no asphaltene in the simulation cell, and then they are no longer placed in the range of adsorption (> 12 Å). This could also be considered as an acceptable performance of the designed simulation cell.

3.5. Detachment of asphaltene molecule from rock surfaces under the influence of different ions
The distance between the asphaltene molecule and the carbonate and sandstone surfaces was changed by the addition of different ions. In this study, the ion strengths were kept constant to ensure that all the simulation conditions were comparable.

Adding SO_4^{2-} and Na^+ ions to the simulation cell changed the distances of asphaltene from the carbonate and sandstone surfaces to 22.1 Å and 10.4 Å, respectively. Table 8 provides the detachment information of the asphaltene molecule under the effect of common ions in smart water. As shown in table 8, the obtained results highlight the role of cations such as Mg^{2+}, Ca^{2+} and also SO_4^{2-} and HCO_3^- in the cases where carbonate is the rock structure; however, in presence of sandstone surface in the simulation cell, Cl^- and Na^+ play the same role in repelling the used asphaltene molecule in this study. Figure 5 illustrates the detachment of asphaltene molecules under the influence of magnesium ions in the simulation cell for carbonate and silica surfaces using OVITO software (version 3.3.2). The superior role of these ions in facilitating the asphaltene detachment procedure is compatible with the experimental results of this molecular investigation [3].

Similar to the prior results, the detachment distance also has a minimum value for both cases (carbonate and sandstone surfaces), as long as all the ions simultaneously exist in the simulation cells.

4. Conclusion

The atomic analysis in the present work is consistent with the results of an experimental investigation of the influence of ions on the wettability state of carbonate rock [3]. The obtained results show that the lower structural energy of carbonate rock in comparison with that of sandstone surface represents a more stable thermodynamic condition for carbonate surface, so that the repulsive forces are more dominant in the presence

of it in equal conditions (in terms of the number of other present atoms). Hence, it can be highlighted that asphaltene desorption mechanisms occur with more certainty when carbonate is used as the rock type. To summarize, the following are the highlighted points of the simulations:

- The maximum non-bonding energy belongs to sulfate and hydrogen bicarbonate ions in the carbonate surface, whereas in the sandstone surface, chlorine and sodium ions dedicated the maximum values of non-bonding energy to themselves.

- The Coulomb interaction outlines a thermodynamically balanced condition with stronger repulsive forces on the carbonate surface than on the sandstone surface.

- The wide ion distribution along the simulation cell for carbonate shows better dissolution of ions and, as a result, better interaction with asphaltene and rock structures.

- The changes in the angle between the center of mass of the asphaltene and the rock surface do not follow any regular pattern, which could be due to the Brownian motion of water molecules and their impact on the asphaltene angle.

- The existence or absence of asphaltene molecules affects the ion density along the simulation cell, so that the affinity between the asphaltene molecule and different ions takes more ions out of the range of interaction with the rock surfaces.

All procedures performed in studies involving human participants were in accordance with the ethical standards of the institutional and/or national research committee and with the 1964 Helsinki Declaration and its later amendments or comparable ethical standards.

The original contributions presented in the study are included in the article/supplementary material, further inquiries can be directed to the corresponding author/s.

The authors declare that they have NO affiliations with or involvement in any organization or entity with any financial interest in the subject matter or materials discussed in this manuscript.

Data availability statement

All data that support the findings of this study are included within the article (and any supplementary files).

ORCID iDs

Pouyan Ahmadi ⬥ https://orcid.org/0000-0002-5452-1560
Hamidreza Asaadian ⬥ https://orcid.org/0000-0002-4824-2899

References

[1] Xie Q *et al* 2014 Ions tuning water flooding experiments and interpretation by thermodynamics of wettability *Journal of Petroleum Science and Engineering.* **124** 350–8
[2] Hassenkam T *et al* 2011 Pore scale observation of low salinity effects on outcrop and oil reservoir sandstone *Colloids Surf., A* **390** 179–88
[3] Ahmadi P *et al* 2019 A new approach for determination of carbonate rock electrostatic double layer variation towards wettability alteration *J. Mol. Liq.* **275** 682–98
[4] Maghsoudian A *et al* 2020 Direct insights into the micro and macro scale mechanisms of symbiotic effect of SO42−, Mg2+, and Ca2 + ions concentration for smart waterflooding in the carbonated coated micromodel system *J. Mol. Liq.* **315** 113700
[5] Shirazi M, Kord S and Tamsilian Y 2019 Novel smart water-based titania nanofluid for enhanced oil recovery *J. Mol. Liq.* **296** 112064
[6] Morrow N and Buckley J 2011 Improved oil recovery by low-salinity waterflooding *Journal of Petroleum Technology.* **63** 106–12
[7] Su W *et al* 2019 New insights into the mechanism of wettability alteration during low salinity water flooding in carbonate rocks *J. Dispersion Sci. Technol.* **40** 695–706
[8] Busireddy C and Rao D N 2004 Application of DLVO theory to characterize spreading in crude oil-brine-rock systems *SPE/DOE Symposium on Improved Oil Recovery. Society of Petroleum Engineers*
[9] Ahmadi P, Riazi M and Malayeri M R 2017 Investigation of wettability alteration of carbonate rock in presence of sulfate, calcium, and magnesium ions (Austria: International Symposium of the Society of Core Analysts held in Vienna) 27–30 August
[10] Kuznetsov D. *et al* 2015 Low-salinity waterflood simulation: mechanistic and phenomenological models *SPE Asia Pacific enhanced oil recovery conference. Society of Petroleum Engineers*
[11] Ligthelm D J *et al* 2009 Novel Waterflooding Strategy By Manipulation Of Injection Brine Composition *EUROPEC/EAGE conference and exhibition. Society of Petroleum Engineers*
[12] McGuire P *et al* 2005 Low salinity oil recovery: An exciting new EOR opportunity for Alaska's North Slope *SPE western regional meeting. Society of Petroleum Engineers*

[13] Sohrabi M *et al* 2017 Novel insights into mechanisms of oil recovery by use of low-salinity-water injection *SPE J.* **22** 407–16

[14] Lee S Y *et al* 2010 Low salinity oil recovery: increasing understanding of the underlying mechanisms *SPE improved oil recovery symposium. Society of Petroleum Engineers*

[15] Shabib-Asl A, Ayoub M and Elraies K 2015 Laboratory investigation into wettability alteration by different low salinity water compositions in sandstone rock *SPE/IATMI Asia Pacific Oil & Gas Conf. and Exhibition. Society of Petroleum Engineers*

[16] Ding H and Rahman S 2017 Experimental and theoretical study of wettability alteration during low salinity water flooding-an state of the art review *Colloids Surf., A* **520** 622–39

[17] Shirazi M *et al* 2020 Smart water spontaneous imbibition into oil-wet carbonate reservoir cores: Symbiotic and individual behavior of potential determining ions *J. Mol. Liq.* **299** 112102

[18] Buckley J and Liu Y 1998 Some mechanisms of crude oil/brine/solid interactions *Journal of Petroleum Science and Engineering.* **20** 155–60

[19] Buckley J 1998 *Evaluation of reservoir wettability and its effect on oil recovery. Annual report, February 1, 1996–January 31, 1997* (Socorro, NM: New Mexico Inst. of Mining and Technology)

[20] Sayyouh M *et al* 1991 Role of polar compounds in crude oils on rock wettability *Journal of Petroleum science and Engineering.* **6** 225–33

[21] Toulhoat H and Lecourtier J 1991 *Physical Chemistry of Colloids and Interfaces in Oil Production: Proc. of the 6th IFP Exploration and Production Research Conf., Held in Saint-Raphaël, September 4–6, Vol. 49. 1992: Editions Technip*

[22] Morrow N R 1990 Wettability and its effect on oil recovery *Journal of Petroleum Technology.* **42** 1

[23] Bryant E, Bowman R and Buckley J 2006 Wetting alteration of mica surfaces with polyethoxylated amine surfactants *Journal of Petroleum Science and Engineering.* **52** 244–52

[24] Morrow N 1998 Evaluation of reservoir wettability and its effect on oil recovery-Preface (Netherlands: Elsevier Science)

[25] Speight J G 2006 *The Chemistry and Technology of Petroleum* 4th edn (Boca Raton, FL: CRC Press) (https://doi.org/10.1201/9781420008388)

[26] Asaadian H, Soltani Soulgani B and Karimi A 2017 An experimental study on electrical effect on asphaltene deposition *Pet. Sci. Technol.* **35** 2255–61

[27] Joonaki E *et al* 2019 Water versus asphaltenes; liquid–liquid and solid–liquid molecular interactions unravel the mechanisms behind an improved oil recovery methodology *Sci. Rep.* **9** 1–13

[28] Groenzin H and Mullins O C 2000 Molecular size and structure of asphaltenes from various sources *Energy & Fuels.* **14** 677–84

[29] Leontaritis K, Amaefule J and Charles R 1994 A systematic approach for the prevention and treatment of formation damage caused by asphaltene deposition *SPE Production & Facilities.* **9** 157–64

[30] Aghajanzadeh M R and Sharifi M 2019 Stabilizing silica nanoparticles in high saline water by using polyvinylpyrrolidone for reduction of asphaltene precipitation damage under dynamic condition *Chin. J. Chem. Eng.* **27** 1021–9

[31] Franco C A *et al* 2013 Nanoparticles for inhibition of asphaltenes damage: adsorption study and displacement test on porous media *Energy & Fuels.* **27** 2899–907

[32] Dubey S and Waxman M 1991 Asphaltene adsorption and desorption from mineral surfaces *SPE Reservoir Engineering.* **6** 389–95

[33] Pernyeszi T *et al* 1998 Asphaltene adsorption on clays and crude oil reservoir rocks *Colloids Surf., A* **137** 373–84

[34] Collins S and Melrose J 1983 Adsorption of asphaltenes and water on reservoir rock minerals *SPE Oilfield and Geothermal Chemistry Symp.. Society of Petroleum Engineers*

[35] Shayan N N and Mirzayi B 2015 Adsorption and removal of asphaltene using synthesized maghemite and hematite nanoparticles *Energy & Fuels.* **29** 1397–406

[36] Nassar N N *et al* 2015 A new model for describing the adsorption of asphaltenes on porous media at a high pressure and temperature under flow conditions *Energy & Fuels.* **29** 4210–21

[37] Nassar N N, Hassan A and Pereira-Almao P 2011 Comparative oxidation of adsorbed asphaltenes onto transition metal oxide nanoparticles *Colloids Surf., A* **384** 145–9

[38] Nassar N N, Hassan A and Pereira-Almao P 2011 Effect of the particle size on asphaltene adsorption and catalytic oxidation onto alumina particles *Energy & Fuels.* **25** 3961–5

[39] Martins Ed F *et al* 2019 Uncovering the Mechanisms of Low-Salinity Water Injection EOR Processes: A Molecular Simulation Viewpoint *Offshore Technology Conf. Brasil. Offshore Technology Conf.*

[40] Chávez-Miyauch T E, Lu Y and Firoozabadi A 2020 Low salinity water injection in Berea sandstone: Effect of wettability, interface elasticity, and acid and base functionalities *Fuel.* **263** 116572

[41] Song J *et al* 2020 Effect of salinity, Mg2 + and SO42− on 'smart water'-induced carbonate wettability alteration in a model oil system *J. Colloid Interface Sci.* **563** 145–55

[42] Naeem M H T and Dehaghani A H S 2020 Evaluation of the performance of oil as a membrane during low-salinity water injection; focusing on type and concentration of salts *Journal of Petroleum Science and Engineering* **192** 107228

[43] Yang G *et al* 2015 Desorption mechanism of asphaltenes in the presence of electrolyte and the extended Derjaguin–Landau–Verwey–Overbeek theory *Energy & Fuels.* **29** 4272–80

[44] Ahmadi P. *et al* 2021 Experimental investigation of different brines imbibition influences on co-and counter-current oil flows in carbonate reservoirs *Chinese J. Chem. Eng.* **33** 17–29

[45] Mayo S L, Olafson B D and Goddard W A 1990 DREIDING: a generic force field for molecular simulations *J. Phys. Chem.* **94** 8897–909